IEEE Access
Multidisciplinary | Rapid Review | Open Access Journal

Received April 29, 2020, accepted May 15, 2020, date of publication June 1, 2020, date of current version June 11, 2020.

Digital Object Identifier 10.1109/ACCESS.2020.2998926

Completed Extremely Nonnegative DMD for Color Texture Classification

MINGXIN JIN, YONGSHENG DONG, (Senior Member, IEEE), MINGCHUAN ZHANG, (Member, IEEE), QINGTAO WU, LINTAO ZHENG, BIN SONG, LEI ZHANG, AND LIN WANG

School of Information Engineering, Henan University of Science and Technology, Luoyang 471023, China

Corresponding author: Yongsheng Dong (dongyongsheng98@163.com)

This work was supported in part by the Key Specialized Research and Development Breakthrough of Henan Province under Grant 192102210121, Grant 192102210130, and Grant 202102210169, in part by the Program for Science and Technology Innovation Talents in Universities of Henan Province under Grant 19HASTIT026, in part by the Key Science and Technology Program of Henan Province under Grant 182102210283, and in part by the Training Program for the Young-Backbone Teachers in Universities of Henan Province under Grant 2017GGJS065.

ABSTRACT Dense micro-block difference (DMD) has achieved good performance in gray texture representation and classification. However, its performance is not satisfactory when representing color texture. To alleviate this problem, we propose a novel color texture representation method based on Completed Extremely Nonnegative DMD (CEN-DMD) in this paper. In particular, we first use DMD to model interchannel features and interchannel features of color texture images. Considering that negative value is meaningless in a digital image, we perform a nonnegative operation during the difference process. Due to that the maximum value in a nonnegative difference patch represents a significant difference, we construct the Extremely Nonnegative DMD (EN-DMD) by fusing the maximum values of the intrachannel features and the maximum of interchannel features, and further build Completed Extremely Nonnegative DMD (CEN-DMD) by fusing EN-DMDs at five scales and the global feature of the color texture images. Finally, the Fisher Vector is used to encode the CEN-DMD to obtain a color texture descriptor. Experimental results on five published standard color texture datasets (CUReT, Colored Brodatz, VisTex, USPTex and KTH-TIPS) reveal that CEN-DMD is effective when compared to the thirteen representative color texture classification methods.

INDEX TERMS Color texture representation, dense micro-block difference (DMD), extremely nonnegative multiresolution, texture classification.

I. INTRODUCTION

Texture classification is a classic problem in the field of pattern recognition and computer vision. How to capture discriminative features from texture images is the key to solving the texture classification problem. Texture analysis and representation are also used in a variety of visual applications such as object recognition [1]–[4], face recognition [5]–[7], video classification [8], [9], image segmentation [10]–[12], and image or video retrieval [13], [14].

Since there is currently no uniform definition of textures, building an effective representation of any given texture image is always a challenging subject. This has also attracted a lot of scholars' attention, and various texture representation methods has been successively proposed. Texture features can be represented by the relationship between neighboring pixels and central pixels in the texture image, which is also referred to as the spatial domain method. The local binary pattern (LBP) is a method of representing a texture image by binarizing the difference between the neighborhood pixels and the center pixel [15]. It is a representative spatial domain method. In recent years, many variants of LBP have also been proposed by improving the deficiencies of the original local binary pattern [16]–[21]. The completed local binary pattern (CLBP) decomposes the image local differences into two components of sign and magnitude by a local difference sign-magnitude transform [22]. In order to enhance the robustness to rotation and noise, binary rotation invariant and

The associate editor coordinating the review of this manuscript and approving it for publication was Donato Impedovo.

noise tolerant (BRINT) [23] and median robust extended LBP (MRELBP) [24] are proposed respectively.

On the other hand, transform domain methods are to model transformation coefficients in the transformed domain. The widely used transform tools include wavelets [25], [26], contourlets [27] and shearlets [28]. Typically, Local energy histogram [25] and Heterogeneous and Incrementally Generated Histogram (HIGH) were proposed to model the wavelet coefficients for texture classification [29]. Poisson mixture model was used to model the contourlet subband coefficients [30]. Linear regression model is used to model the shearlet domain [28].

However, these texture feature extraction methods focus only on gray-scale images and ignore color information. Color is a discriminative information in human vision, and it is also necessary to consider color information when performing texture feature extraction [31], [32]. Extracting discriminative color texture features is also a concern of many scholars who study texture classification. For color texture feature extraction, it is intuitive to use the feature extraction methods of grayscale texture on three color channels [33]. More important is to explore the features between the relative color channels. Junior *et al.* [33] used the theory in the data structure to view each pixel as a vertex in the graph, thereby constructing an undirected graph to represent the three color channels. The statistical moment of the shortest path between specific vertices in the undirected graph is calculated as a color texture feature. Since Improved LBP (ILBP) is conceptually simple, easy to implement and efficient LBP variant, Bianconi *et al.* [34] proposed to use this coding model to extract the features of intrachannels and interchannels for color texture classification. Similarly, transform domain methods are also applicable to color texture images. The analytic Gabor filters were used to analyze the color texture by calculating the first- and second-order statistics of the filtered response and using homomorphic filtering to compensate for illumination changes in the image [35]. In order to better describe the color, Chen *et al.* [36] designed a new color image processing tool called Complementary Color Wavelet Transform (CCWT) to make up for the gap between wavelet and complementary color. A more comprehensive study of color texture analysis can be found in [37], [38]. Furthermore, color texture analysis is also used for texture retrieval [39], pathological image analysis [40] and endoscopic and dermoscopic medical image analysis [35].

Modeling between relative color channels is a powerful trick for texture analysis. However, most of this kind of methods may ignore the global features of color texture. To alleviate this problem, in this paper, we propose a novel Completed Extremely Nonnegative DMD (CEN-DMD) texture descriptor for color texture classification. Particularly, we model color texture images using dense micro-block difference (DMD) to extract dense micro-block difference features of intrachannels and interchannels. Furthermore, the absolute values of differential features are extracted and the corresponding maximum values for the intrachannel differences and interchannel differences are selected. Multiresolution representation of color texture images is achieved by differential between different scales of micro-blocks. We named it Extremely Nonnegative DMD (EN-DMD). Subsequently, since EN-DMD only capture local features of color images, and global features are also essential for texture feature extraction. Therefore, we propose to combine the global information of the color texture image and the EN-DMD to construct an completed extremely nonnegative DMD descriptor. It contains not only intrachannel features and interchannel features, but also local features and global features of color texture. Fisher Vector (FV) is then used to encode the proposed color texture features, and support vector machines (SVM) is used to perform classification tasks. Finally, experimental results on five publicly available color texture datasets reveal the effectiveness of our proposed CEN-DMD.

The contributions of our paper are as follows:

- We construct a nonnegative multiresolution DMD feature for representing texture information. This feature is a multiresolution representation of textures by performing the nonnegative operation and then concatenating micro-block features of difference sizes.
- We use the maximum values of three intrachannel difference features and the maximum values of three interchannel difference features of the color texture image to measure the significance of difference features. Intuitively, the maximum value in nonnegative difference indicates a significant difference. In addition, compared with the directly combine all intrachannel and interchannel difference features, the resulting maximum difference feature has a low dimension.
- We propose a Completed Extremely Nonnegative DMD (CEN-DMD) for representing color textures. The complete property of CEN-DMD consists of the intrachannel and interchannel information, as well as the global and local information of the color texture.
- The classification results on the five published standard texture datasets (Colored Brodatz, VisTex, CUReT, USPTex and KTH-TIPS) demonstrate that our proposed method is effective when compared with other representative color texture classification methods.

The remainder of the paper is organized as follows. Related work is shown in the Section II. In the Section III, we present the proposed Completed Extremely Nonnegative DMD for color texture representation method. Experimental results and comparison about color texture classification are presented in Section IV. Finally, Section V is the conclusion of the paper.

II. RELATED WORK

Building an effective color texture representation is a key step for performing color texture classification. As we all know, we can construct the corresponding descriptor of the three color channels by using gray-scale texture representation method, and further obtain the representation of the

whole color texture image. However, for a color texture image, the three color channels are not independent. Some researchers proposed some modeling methods for building effective color texture representation methods. We now briefly review two representative methods below.

• *Shortest Path in Graph for Color Texture*: In order to explore the relationship among pixels of different color channels, Jarbas *et al.* proposed to model a color texture image as an undirected graph [33]. An image is made up of a number of pixels, each of which can be thought of as a vertex in an undirected graph. An edge connecting two vertices can be constructed between adjacent pixels, and the weight of the edge can be calculated from the pixel value of the pixel corresponding to the connected vertex. Texture features can be obtained by calculating the statistical moments of the shortest path in the undirected graph. For a color texture image, two undirected graphs can be constructed. On is to construct an undirected graph on each color channel. That is to say, a color texture image corresponds to three undirected graphs, so each shortest path belongs to only one color channel. The other is to create an undirected graph representing the entire color image. In other words, the three channels are represented as whole, so that the shortest path can explore the relationship between different color channels.

• *Improved Opponent Color Local Binary Patterns*: As a variant of Local Binary Pattern (LBP), Improved LBP (ILBP) is conceptually simple and easy to implement based on the point-to-average threshold method. Motivated by it, Francesco *et al.* proposed the use of this coding scheme for extracting intrachannel and interchannel features for color texture analysis, known as Improved Opponent Color Binary Patterns (IOCLBP) [34]. A more intuitive description of IOCLBP, the mathematical expression is as follows:

$$F_{IOCLBP} = \sum_{i=0}^{n} 2^i \phi\left(\bar{p}_u, p_{i,v}\right), \tag{1}$$

where

$$\bar{p}_u = \frac{1}{n+1} \sum_{i=0}^{n} p_{i,u}, \tag{2}$$

$$\phi\left(x, y\right) = \begin{cases} 0 & if, x < y \\ 1 & otherwise \end{cases} \tag{3}$$

where $p_{i,v}$ means the intensity of the *ith* pixel in the *vth* channel, n is the number of pixels in the local neighborhood. It can be easily seen from equation (1) and (2) that IOCLBP is capable of capturing intrachannel feature and interchannel feature.

Although these methods achieved good performance in color texture classification, they only focus on local information and ignore the global features of color textures. Therefore, we propose an Completed Extremely Nonnegative DMD (CEN-DMD) for color texture classification. We will describe our proposed CEN-DMD in the following section in detail.

III. OUR PROPOSED COMPLETED EXTREMELY NONNEGATIVE DMD COLOR TEXTURE REPRESENTATION METHOD

In this section, we present the proposed Completed Extremely Nonnegative DMD (CEN-DMD) color texture descriptor. Particularly, we model color texture images by using dense micro-block difference (DMD) to extract dense micro-block difference features of intrachannels and interchannels. Furthermore, the absolute values of differential features are extracted and the corresponding maximum values for the intrachannel differences and interchannel differences are selected. We then present the global feature extraction of the color texture image, followed by the Fisher Vector (FV) encoding, and further we obtain the color descriptor.

A. EXTREMELY NONNEGATIVE DMD

Due to that an image texture was defined as the local spatial variations in pixel intensities and orientation [41], the difference representation is a powerful characteristic for capturing texture information. Furthermore, the individual pixels are more susceptible to noise, the dense micro-block difference in an image patch was proposed to replace the micro-block difference of a single pixel for performing gray-scale texture image classification [42], [43]. To capture local difference information for an image, pairs of micro-blocks in each image patch are used to encode the local structure of the image patch, where the average intensity of the micro-block is considered for capturing variations. In this approach, texture information of a given patch I_p can be captured by utilizing smaller block, named as micro-block, in the patch instead of the individual pixel. In a given image, the pairs of micro-blocks in each image patch are used to encode the local structure of the image patch. Particularly, a given an image patch I_p of size $L \times L$ and two set of sample points $X = \{x_1, x_2, \ldots, x_n\}$ and $Y = \{y_1, y_2, \ldots, y_n\}$, the micro-block difference of patch I_p is defined as:

$$F\left(I_p\right) = \left\{\left|M_s\left(x_1\right) - M_s\left(y_1\right)\right|, \ldots, \left|M_s\left(x_n\right) - M_s\left(y_n\right)\right|\right\}, \tag{4}$$

where

$$M_s\left(a, b\right) = \sum_{i=0}^{s-1} \sum_{j=0}^{s-1} \frac{I_p\left(a+i, b+j\right)}{s^2}, \tag{5}$$

where $M_s\left(x\right)$ is the average intensity of pixel in the micro-block at the position $x^c = (a, b)^T$ in the I_p, s is the size of the micro-block.

Since color images consist of three color channels, building a color texture descriptor is to extract intrachannel features or interchannel features. Intuitively, pairs of micro-blocks from image patches of the same color channel can be used for building intrachannel features. That is to say, the micro-block difference features within the three channels are extracted to capture intrachannel texture information. More challenging and more meaningful is to explore the relationship between color channels and extract interchannel features. We first

select pairs of micro-blocks from image patches of different color channels. Due to that the channel pairs, (u, v) and (v, u) can capture the same texture information, we only use one of them to build the texture descriptor to avoid computational redundancy. Furthermore, we can extract color texture information from the combinations of three color channels.

In the image patch of each color channel of the color texture image, the selection of the pair of micro-blocks is determined by the set of two sample points $X^c = \{x_1^c, x_2^c, \ldots, x_n^c\}$ and $Y^c = \{y_1^c, y_2^c, \ldots, y_n^c\}$, where $c \in \{u, v, w\}$ represents the color channel and n represents the number of sample points. In this paper $n = 80$. For the image patch I_p^c of size $L \times L$ on the c color channel, the intrachannel difference is defined as follows:

$$F\left(I_p^c\right) = \left\{\left|M_s^c\left(x_1^c\right) - M_s^c\left(y_1^c\right)\right|, \ldots, \left|M_s^c\left(x_n^c\right) - M_s^c\left(y_n^c\right)\right|\right\}, \tag{6}$$

where

$$M_s^c(a, b) = \sum_{i=0}^{s-1}\sum_{j=0}^{s-1} \frac{I_p^c(a+i, b+j)}{s^2}, \tag{7}$$

where the size of micro-block is $s \times s$, $x^c = (a, b)^T$ represents the coordinates in the image patch on the special color channel, $M_s^c(x^c)$ is the average intensity of the pixels located in the micro-block of $x^c = (a, b)^T$ and $||$ indicates absolute value operation. Since negative values are meaningless in digital images, we use absolute value operators in differential operations to make the difference features nonnegative. Therefore, the micro-block differences in the three color channels can be extracted.

More meaningful and more challenging is to explore the information between the color channels of a color texture image. Micro-block differences are used to model the relationship between the color channels of a color texture image. In the modeling process, the micro-block pairs are respectively selected from texture image patch of different color channels. In order to avoid the redundancy of calculation, only one of two combinations (u, v) and (v, u) is considered. So that there are three different combinations of color channels. Similarly, the choice of micro-block pairs is determined by the set of sample points X^c and Y^c. For the patch of size $L \times L$, the interchannel difference are expressed as follows:

$$F\left(I_p^{c-c'}\right) = \left\{\left|M_s^c\left(x_1^c\right) - M_s^{c'}\left(y_1^{c'}\right)\right|, \ldots, \left|M_s^c\left(x_n^c\right) - M_s^{c'}\left(y_n^{c'}\right)\right|\right\}, \tag{8}$$

where $I_p^{c-c'}$ is the interchannel difference of image patch between c color channel and c' color channel, $c \in \{u, v, w\}$ and $c' \in \{u, v, w\}$. Fig. 1 shows the process of extracting intrachannel and interchannel dense micro-block difference.

The choice of micro-block pairs plays an important role in the process of feature extraction. The student t-distribution $i.e.(X, Y) \sim i.i.d.t(\sqrt{L})$ is used to sample the micro-block in the image patch. That is to say, to generate sample points in set X^c and Y^c. It is well known that the tail of the t-distribution

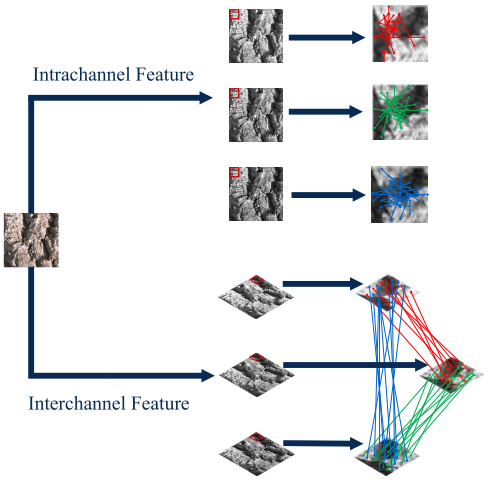

FIGURE 1. The extraction process of micro-block difference of color texture including Intrachannel difference and Interchannel difference. The Intrachannel difference refer to capturing micro-block difference within a single color channel. The Interchannel difference explores the relationship between two different color channels.

is higher than the Gaussian distribution, and it is possible to capture relatively more edge information of the image block for selecting the micro-block in the image patch. The sampling points on the three color channels are different, and thus the distance or angle between the pair of micro-blocks in a single color channel or between color channels is not a constant. So this will lead to capture multi-scale information and more direction information in the image patch. We select a set of sample points in the set for selecting the pair of micro-blocks, and calculate the distance and consine between the sample points. Fig. 2 and Fig. 3 show the distribution histograms of distance and cosine values, respectively. We can see from Fig. 2 that the distance of the sampling points is not a specific constant. That is to say, the micro-block difference can capture different scales information. Correspondingly, It can be seen from Fig. 3 that the direction of the sampling point is not a fixed value, and thus the above micro-block difference can capture the texture information in different directions.

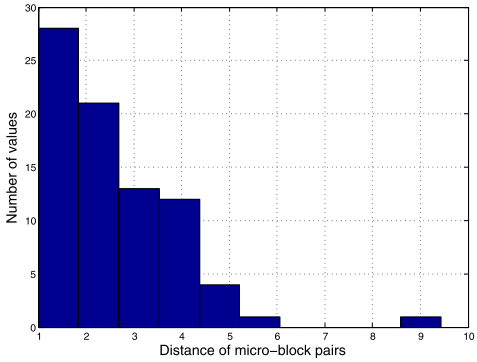

FIGURE 2. Histogram of distances of micro-block pairs.

Intuitively, the maximum value of a given set indicates a significant characteristic of the set. Moreover, negative numbers are meaningless in digital images when performing

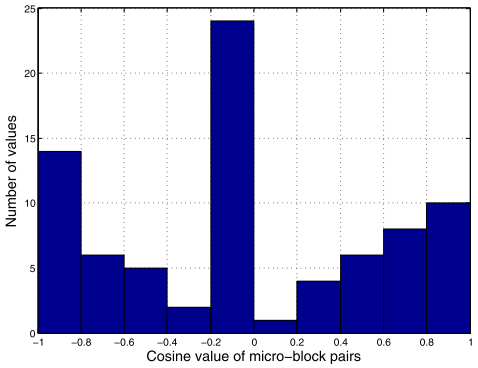

FIGURE 3. Histogram of cosine values of micro-block pairs.

differential modeling, and thus we construct a nonnegative dense micro-block difference for further representing texture information. However, the features obtained by directly concatenating intrachannel features and interchannel features will cause the dimension of the feature to be too large. So we aim at using the maximum values of three intrachannel difference features and the maximum values of three interchannel difference features of the color texture image to measure the significance of difference features, and further combine intrachannel feature with interchannel feature as a whole for color texture analysis. At the same time, we can select different sizes of micro-blocks for differentiation and capture multiresolution information of color textures. We call this combined feature an Extremely Nonnegative DMD, abbreviated as EN-DMD. The EN-DMD is defined as follows:

$$\text{EN-DMD} = \left[\max\left(F\left(I_p^u\right), F\left(I_p^v\right), F\left(I_p^w\right)\right), \max\left(F\left(I_p^{u-v}\right), F\left(I_p^{v-w}\right), F\left(I_p^{w-u}\right)\right)\right]. \tag{9}$$

Note that in this paper, we use RGB color space for color texture analysis. The RGB color space based on the three basic colors of red, green and blue can be superimposed to different degrees to produce a rich and wide color. Since it is close to a nature color, the RGB color space is also a nature color mode [44].

For clarity, we randomly select two sample images from two different texture classes in the VisTex texture dateset. Fig. 4 shows the two texture images from the VisTex dataset and their dense micro-block difference histograms. In the sub-figures of Fig. 4, the x-axis of the sub-figure represents the distribution range of the difference feature, and the y-axis represents the frequency. In the histogram, each bin represented by a different color. Fig. 4(c) and (d) show their histograms of intrachannel and interchannels dense micro-block differences. Fig. 4(e) and (f) show their histogram of the maximum values of three intrachannel dense micro-block differences and the maximum values of three interchannel dense micro-block differences. That is to say, the histograms are obtained by using our proposed EN-DMD. It can be easily seen from Fig. 4 that the two histograms (c) and (d) have

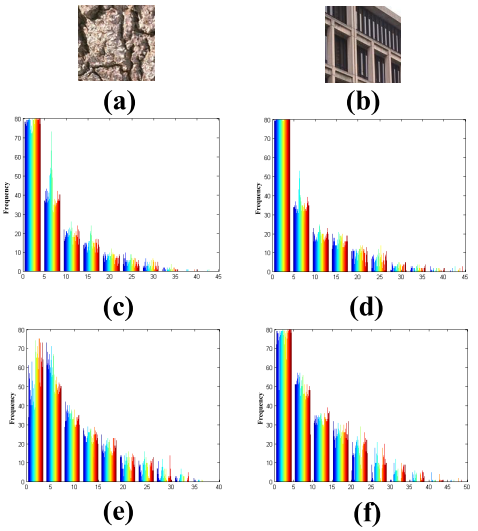

FIGURE 4. Two texture images from the VisTex dataset and their difference histograms. (a) Bark. 0009, (b) Buildings. 0002, (c) Histograms of Interchannel and Intrachannels differences of texture Bark. 0009, (d) Histograms of Interchannel and Intrachannels differences of texture Buildings. 0002. (e) Histogram of the maximum values of three intrachannel differences and the maximum values of three interchannel differences corresponding to texture Bark. 0009. (f) Histogram of the maximum values of three intrachannel differences and the maximum values of three interchannel differences corresponding to texture Buildings. 0002.

similar distributions, and thus the two corresponding texture classes can not easily be distinguished by using these two histogram features. However, the two histogram (e) and (f) are obviously different, and thus we can distinguish these two textures by our proposed EN-DMD.

B. GLOBAL FEATURE EXTRACTION OF COLOR TEXTURE IMAGE

The EN-DMD not only contains intrachannel features but also interchannel features. However, EN-DMD only captures local features of color texture without considering the global features of color texture image. Global features are also indispensable as an important component of texture features. To compensate for this deficiency, we combine local texture features and global features to form a Completed Extremely Nonnegative DMD (CEN-DMD). CEN-DMD can not only capture the intrachannel features and interchannel features of color texture, but also capture local features and global features of color texture. Similar to capturing local features, global features can also be divided into intrachannel global features and interchannel global features. Intuitively, we use the average and variance of the pixels in a single color channel as an intrachannel global features. For the interchannel global features, we make the difference between the pixels of different color channels, and the mean and variance of the pixel difference as the global features between the channels. The color texture image I, I_R, I_G and I_B represent image information on the three color channels, respectively. The intrachannel global features are $avg(I_R)$, $avg(I_G)$, $avg(I_B)$ and

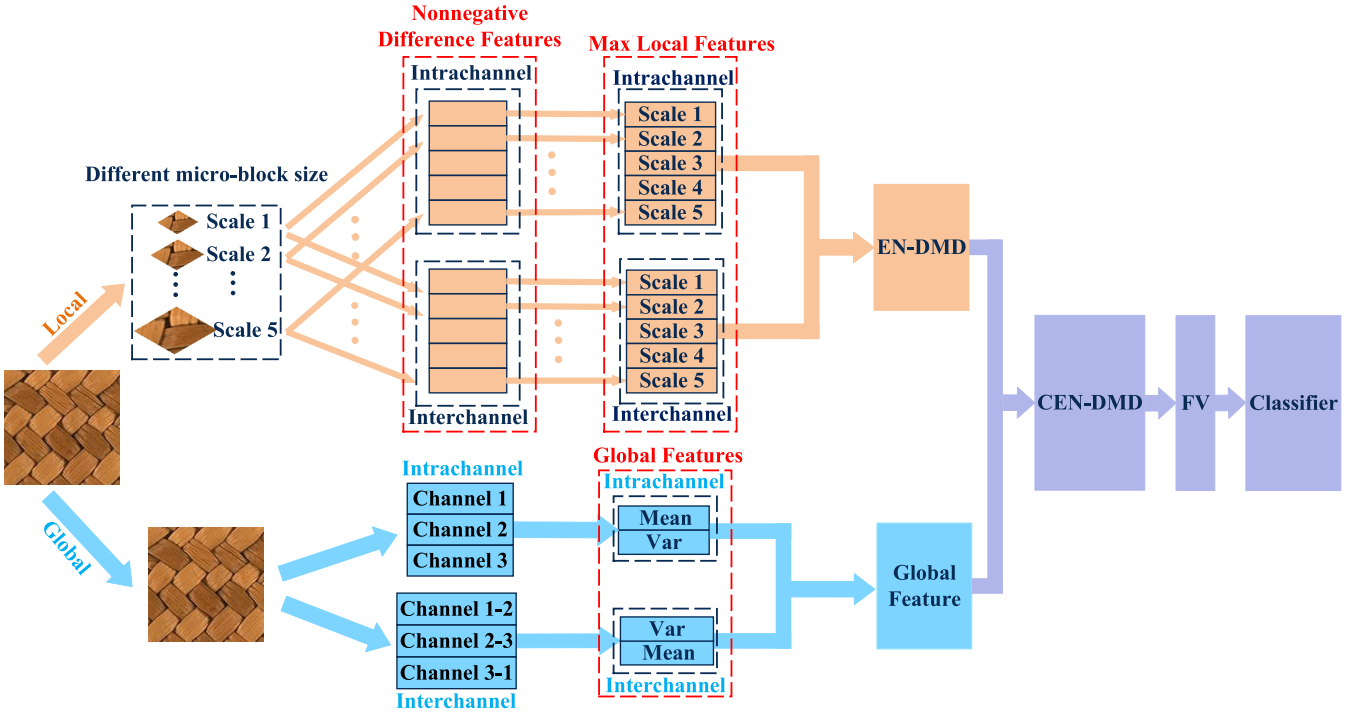

FIGURE 5. The flowchart of the proposed method of color texture feature extraction. (1) Extracting the patch at intervals of two pixels in the original color texture images, (2) Modeling the color texture image with DMD, extracting intrachannel features and interchannel features, combining the maximum value of three intrachannel features and the maximum value of three interchannel features to construct EN-DMD, (3) Capturing the global features of the color images and constructing the CEN-DMD in combination with EN-DMD, (4) The Fisher Vector encoding the CEN-DMD to obtain a color texture descriptor, (5) The SVM is used to perform classification tasks.

$var(I_R)$, $var(I_G)$, $var(I_B)$ and the intrachannel global features G_{Intra} is defined as follows:

$$G_{Intra} = [avg\,(I_R)\,, avg\,(I_G)\,, avg\,(I_B)\,, var(I_R), var\,(I_G)\,, var\,(I_B)]\,. \quad (10)$$

Next the interchannel global features are $avg(|I_R - I_G|)$, $avg(|I_G - I_B|)$, $avg(|I_B - I_R|)$ and $var(|I_R - I_G|)$, $var(|I_G - I_B|)$, $var(|I_R - I_G|)$ and the interchannel global features G_{Inter} is defined as follows:

$$G_{Inter} = [avg\,(|I_R - I_G|)\,, avg\,(|I_G - I_B|)\,, avg\,(|I_B - I_R|)\,, var(|I_R - I_G|), var\,(|I_G - I_B|)\,, var\,(|I_B - I_R|)]\,. \quad (11)$$

Finally, the Completed Extremely Nonnegative DMD (CEN-DMD) is defined as follows:

$$\text{CEN-DMD} = [EN - DMD, G_{Intra}, G_{Inter}]\,, \quad (12)$$

For a given color texture image, our proposed descriptor CEN-DMD not only contains intrachannel features and interchannel features, but also can capture the local features and global features of color image. The completeness of CEN-DMD is also reflected here.

C. FISHER VECTOR ENCODING TO CONSTRUCT A COLOR DESCRIPTOR

In this subsection, we employ Fisher Vector (FV) to refine the above CEN-DMD and obtain the final color texture descriptor. Quantization/hard assignment was used by most early texture classification tasks, but it may lead to a quantization error. As a soft quantization, the Fisher Vector has been used to encode texture features in recent years. In the process of Fisher Vector encoding, a Gaussian mixture model is used for the probability distribution of the original features. The robust representations of the encoding is obtained by capturing the first and second order differences between the image descriptor and the GMM center. The Expectation Maximization (EM) is used to learn the training samples to obtain the parameters of the GMM. For a more detailed discussion of the Fisher Vector, please refer to [45] and [46]. After Fisher Vector encoding, we get a color texture descriptor for the color texture classification task. For simplicity, we still denote the resulting color texture descriptor by CEN-DMD.

The flow chart of our proposed color texture representation method is shown in Fig. 5. The features of the color texture image include two parts, a local feature and global feature. The local features consist of maximum values of three local intrachannel features and the maximum values of three local interchannel features. Multi-resolution representation is achieved by selecting micro-blocks of different scales. We named the Extremely Nonnegative DMD (EN-DMD). Since EN-DMD ignores the global features of color texture images, we combine EN-DMD and global features into a Completed Extremely Nonnegative DMD (CEN-DMD), followed by Fisher Vector encoding. Finally, a linear SVM

classifier is used to perform color texture classification. We will verify the effectiveness of our proposed method by performing a texture classification task in the following section.

IV. EXPERIMENTAL RESULTS

In this section, we perform color texture classification on five public color texture datasets to demonstrate the effectiveness of our proposed Completed Extremely Nonnegative DMD (CEN-DMD), and compared it with the other thirteen representative color texture classification methods. For local feature extraction of color texture images, we crop patches for computing local features in 2 pixel steps. The number of sampling points n in the patch is set to 80. The classification accuracy rate is calculated by 10-fold cross-validation.

In our experiments, five standard publicly available color texture datasets are used to verify the performance of our proposed CEN-DMD. The first one is Colored Brodatz as an extension of the original Brodatz from gray-scale to color texture image. It not only contains the rich texture features of the original Brodatz but also rich color information. We selected 40 representative texture classes from 112 texture classes in Colored Brodatz to verify the effectiveness of our proposed method. The samples of Color Brodatz are shown in Fig. 6, each 640×640 texture image is divided into 16 nonoverlapping samples of 160×160, which 8 samples are used for training and 8 samples for testing. The second is the VisTex texture dataset, which is a challenging dataset because it contains real-world texture images. In the experiment, we randomly select 40 texture classes. As shown in Fig. 7, each image of 512×512 is split into 16 nonoverlapping samples of 128×128, among which 8 images are used for training and 8 images for testing. The third is that CUReT contains 61 categories, which are composed of images taken various angles of view and illumination angles. The samples of CUReT are shown in Fig. 8. Each class contains 92 samples, of which 46 samples are used for training and the remaining 46 samples for testing. Because different illumination conditions can cause intra-class variation in appearance, it is a challenging texture dataset for classification. The third is that USPTex contains 191 classes of real-world texture images, each with 12 samples, as shown in Fig. 9, with 6 samples for training and 6 samples for testing. The last one is KTH-TIPS, as shown in Fig. 10, which consists of 10 texture categories, each with 81 samples, including changes in illumination, pose and scale. We used 40 samples for training and the remaining 41 samples for testing. The same classed are used for performing comparison with other color descriptors. The classification accuracy of all descriptors used in experiments is obtained through 10-cross validation.

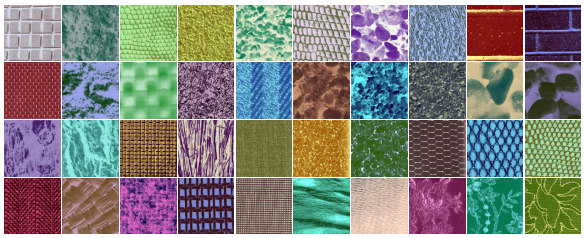

FIGURE 6. Examples of 40 texture classes of Colored Brodatz.

FIGURE 7. Examples of 40 texture classes of VisTex.

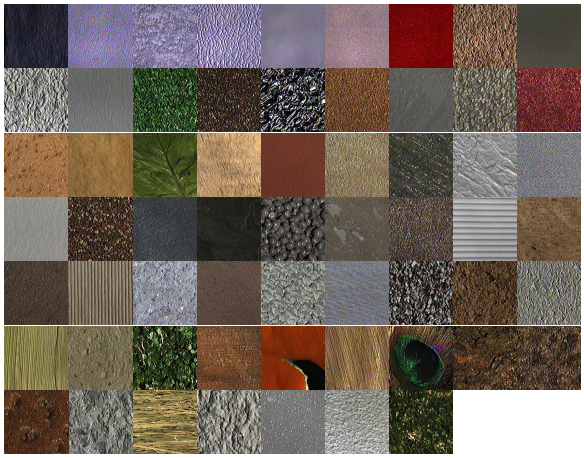

FIGURE 8. Examples of 61 texture classes of CUReT.

A. PARAMETER SENSITIVITY INVESTIGATION AND PERFORMANCE EVALUATION

1) PATCH SIZE

In the process of micro-block difference modeling, the size of the patch and the size of the micro-block are interdependent. If the size of patch is too small, it would lead to repetitive overlap of the micro-blocks, which will capture redundant and correlated features. On the other hand, if the size of patch is too large, the sampling of the micro-block would not insufficient, and the local structure of the texture cannot be effective captured. Therefore, the size of patch is varied from 9×9 to 15×15 with a step size of 2 and the micro-block size is varied from 1 to 5. In addition, the patch size is similar to the settings in the experiments in [42] and [43]. We test changes in experimental results for different parameters. The size of the patch is from 9×9 to 15×15 in steps of 2, and the size of the micro-block is from 1×1 to 5×5. The experiment is performed on the CUReT texture datset, and the experimental results are shown in Table 1. It can be seen from Table 1 that the classification accuracy rate almost increases with the increasing of the size of patches. The highest classification accuracy rate can almost be obtained when the patch size is

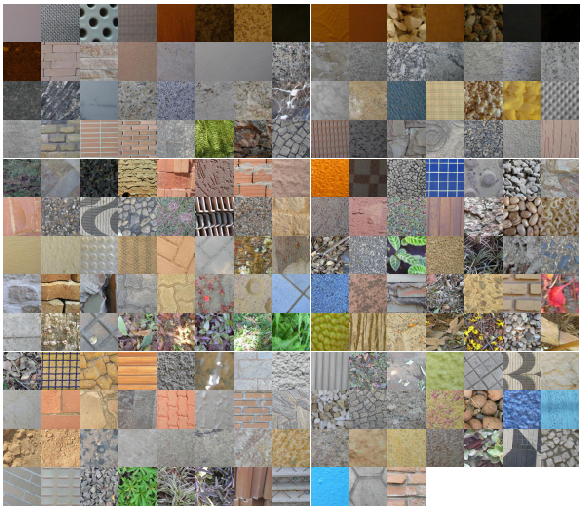

FIGURE 9. Examples of 191 texture classes of USPTex.

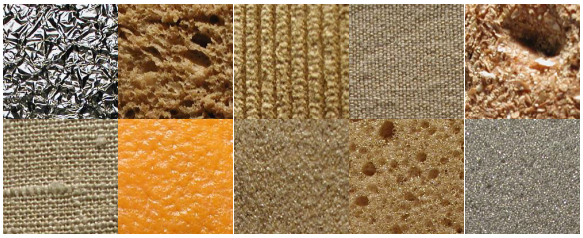

FIGURE 10. Examples of 10 texture classes of KTH-TIPS.

TABLE 1. The classification accuracy rates (%) of different size on the CUReT dataset.

	Patch Size			
Micro-block Size	9×9	11×11	13×13	15×15
1×1	**98.94**	98.93	98.89	98.87
2×2	98.90	98.93	**99.00**	98.95
3×3	98.87	98.96	98.93	**99.01**
4×4	98.87	98.96	99.04	**99.04**
5×5	98.91	98.92	99.02	**99.02**

15 × 15. So we use 15 × 15 as the patch size in the following experiments.

2) MULTIRESOLUTION ANALYSIS

The classification accuracy rate is different under different sizes of micro-blocks, so we can connect different sizes of micro-block to achieve multiresolution representation of texture. The number of sampling points in the patch is 80. When performing multiresolution representation, we connect the micro-block size from 1 × 1 to 5 × 5, which means that the number of micro-blocks per size is 16. We compare it to the single-scale micro-block size 5 × 5, and the experimental results on the four texture datasets are shown in Fig. 11. It is report that a single-scale and multi-scale comparison when the patch is 15 × 15. From the histogram, we can intuitively see that the multi-scale classification performance is better than the single-scale on the four different texture

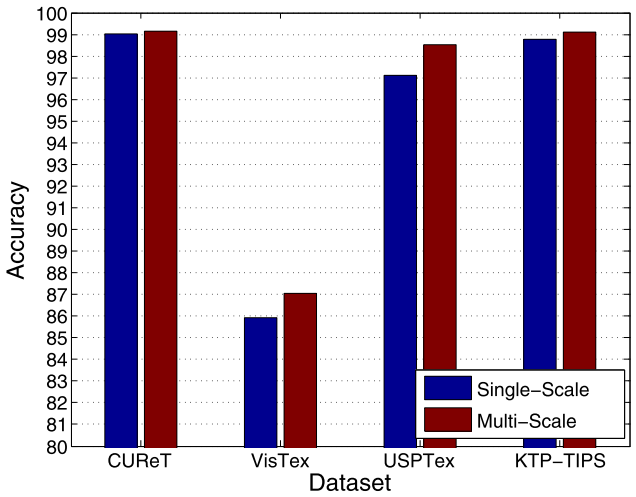

FIGURE 11. The classification accuracy rates (%) of Single-scale and multi-scale on the four texture datasets.

datasets of CUReT, VisTex, USPTex and KTH-TIPS. Especially on USPTex, the multi-scale classification accuracy rate is 1% higher than the single-scale classification accuracy rate. In summary, multiresolution analysis of color textures by connecting different sizes of micro-blocks can capture more detailed color texture information. Therefore, we select a multiresolution representation with a micro-block size from 1 × 1 to 5 × 5 in the following experiments.

3) NUMBER OF GAUSSIAN COMPONENTS

The Gaussian mixture model is used to fit the distribution of the original feature in the Fisher Vector. The number of Gaussian components is an important parameter in the Fisher Vector coding process. Similar to Mehta and Eguiazarian [42], in order to better fit the original features, we selected a different number of components from 16 to 128 and experimented on three texture datasets. The experimental results are shown in Table 2, the classification accuracy rate on the three datasets increases as the number of Gaussian components increases. According to the experimental results, we selected 128 Gaussian components in the Fisher Vector encoding process.

TABLE 2. The classification accuracy rates (%) with different number of gaussian component on the three texture datasets.

	The number of GMM compoments				
Dataset	16	32	64	96	128
VisTex	83.56	84.25	85.94	86.44	**86.91**
USPTex	97.55	97.83	98.41	98.46	**98.53**
KTH-TIPS	98.20	98.56	98.83	98.85	**98.95**

4) COLOR SPACE

In the following experiment, we investigate the sensitivity of color space to color texture classification performance. We test the classification performance of CEN-DMD on three

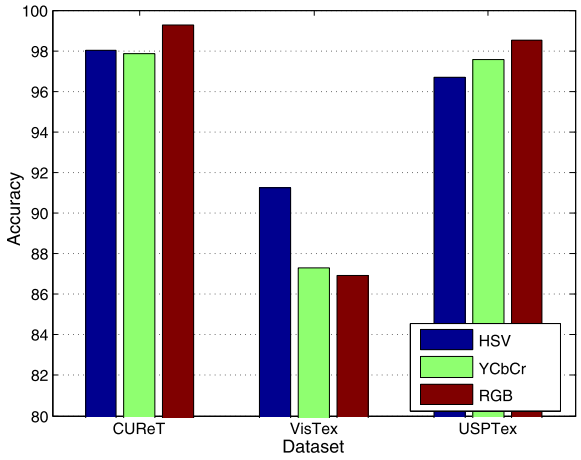

FIGURE 12. The classification accuracy rates (%) of CEN-DMD on the three texture datasets in three different color spaces.

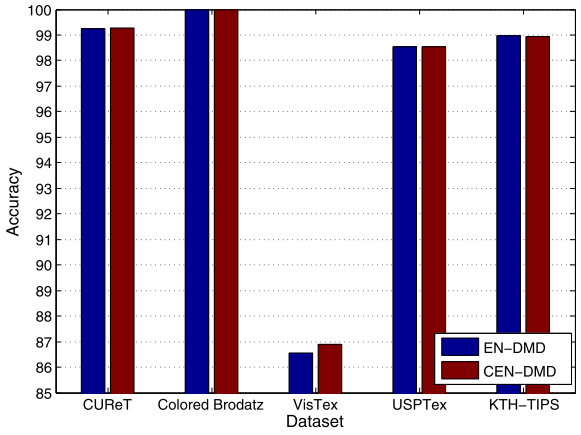

FIGURE 13. The classification accuracy rates (%) of CEN-DMD and EN-DMD on the five color texture datasets.

texture datasets in three color space: RGB, HSV and YCbCr. The classification performance in different color space is shown in Fig. 12. Fig. 12 shows the classification of three texture datasets in different color spaces. This is because the classification accuracy in different color space on the CUReT, VisTex and USPTex datasets are quite different, which is more intuitive when displayed through histograms and is convenient for readers to read. However, the difference of classification accuracy in different color spaces is not obvious on the Colored Brodatz and KTH-TIPS datasets. Therefore, we choose the classification accuracy on the three datasets for display. Although the classification performance in the RGB color space on the VisTex texture dataset is not optimal, this may be because the heterogeneity of RGB color information of the sample picture in VisTex is weak, and thus the color distributions of picture in VisTex is relatively even. So the RGB color is not good for the VisTex dataset. The classification accuracy rate in the RGB color space on the CUReT and USPTex datasets are the best. In summary, we chose the RGB color space in the experiment.

B. EN-DMD VS CEN-DMD

As we have considered, the Extremely Nonnegative DMD (EN-DMD) extracts only the local features of intrachannel and the local features of interchannels in the color texture image, while ignoring the global features of the color texture image. To this end, we propose to combine the global features of the difference local features and the color texture image into a Completed Extremely Nonnegative DMD (CEN-DMD) for color texture analysis. We selected the patch size to be 5×5 and the micro-block size from 1×1 to 5×5 to compare the performance of EN-DMD and CEN-DMD on five texture datasets. The experimental results are shown in the histogram plotted in Fig. 13, and we can intuitively see that the classification performance of the color texture descriptor is not reduced after the global feature is added. The classification performance of EN-DMD and CEN-DMD on Colored Brodatz, USPTex and KTH-TIPS is comparable. The performance of CEN-DMD is slightly better on CUReT. Especially in the VisTex texture dataset, the classification result of CEN-DMD is significantly better than EN-DMD.

C. COMPARISONS WITH OTHER METHODS

In this subsection, to further validate the effectiveness of our proposed CEN-DMD. We compare the thirteen representative color texture classification methods on five color texture datasets, respectively CUReT, Colored Brodatz, VisTex USPTex and KTH-TIPS. These color texture classification methods are namely Improved oppenent colour local binary pattern (IOCLBP) [34], Extended color local mapped pattern (ECLMP) [47], Multichannel decoded local binary patterns (mdLBP) [48], Local binary pattern + Local colour contrast (LBP + LCC) [49], Local color vector local binary patters (LCVBP) [50], Multilayer coordinated cluster representation (Multilayer CCR) [51], Dual tree complex wavelet transform (DT-CWT) [52], Opponent colour local binary patterns (OCLBP) [53], Integrative co-occurrence matrices (ICM) [54], Rotation invariant of Integrative co-occurrence matrices (ICM^{DFT}) [54] and Opponent Gabor features (OGF) [55]. For calibration purposes, the mean of the R, G and B color channels (Mean) [56], the mean and standard deviation of each color channel (Mean + Std) [56], are used to compare with CEN-DMD. The classification accuracy rates are shown in Table 3.

The CUReT texture dataset contains changes in texture image at different viewing and illumination. It can be seen from Table 3 that the classification accuracy rates of most of the comparison methods can reach 90%, and IOCLBP is the best one among the thirteen competitive methods. Compared with other classification methods, CEN-DMD has the highest classification accuracy rate on CUReT, which is about 1.5% higher than the IOCLBP. Colored Brodatz extends color

TABLE 3. The classification accuracy rates (%) of fifteen color texture representation methods on the five texture datasets.

	CUReT	Colored Brodatz	VisTex	USPTex	KTH-TIPS
IOCLBP [34]	97.89(0.33)	99.94(0.13)	78.19(3.31)	92.30(2.14)	96.44(1.87)
ECLMP [47]	89.79(1.16)	96.22(1.12)	70.34(3.48)	81.36(2.68)	91.98(2.49)
mdLBP [48]	93.84(0.56)	99.85(0.22)	83.38(2.97)	93.27(1.30)	95.37(2.21)
LBP+LCC [49]	91.20(1.30)	98.41(0.96)	75.22(3.06)	83.94(2.27)	93.54(2.92)
LCVBP [50]	97.65(0.38)	99.13(0.69)	79.25(2.50)	91.93(2.20)	96.22(0.93)
Multilayer CCR [51]	72.16(2.03)	99.44(0.55)	65.22(3.65)	69.34(2.68)	88.98(1.75)
DT-CWT [52]	—	98.69(0.66)	64.88(2.77)	80.70(3.16)	—
OCLBP [53]	91.66(0.34)	99.97(0.10)	75.66(4.15)	89.72(2.13)	95.15(2.31)
ICM [54]	92.52(0.72)	99.78(0.26)	70.84(2.89)	87.77(2.54)	92.71(1.42)
ICM^{DFT} [54]	91.94(0.93)	99.91(0.21)	71.38(2.50)	86.00(2.13)	93.39(1.66)
OGF [55]	46.91(0.89)	70.94(1.38)	39.56(1.61)	27.52(1.65)	64.95(1.35)
Mean [56]	54.56(1.97)	96.25(1.20)	38.28(3.33)	33.42(1.84)	94.27(0.91)
Mean+Std [56]	71.40(1.99)	99.13(0.60)	54.56(3.50)	60.85(2.74)	91.59(1.56)
EN-DMD	99.24(0.33)	100.00(0)	86.56(2.21)	98.53(0.98)	**98.98(1.02)**
CEN-DMD	**99.28(0.30)**	**100.00(0)**	**86.91(2.44)**	**98.53(0.92)**	98.95(1.02)

information based on the original Brodatz's rich texture. It can be seen from Table 3 that the most methods can achieve higher classification accuracy rate. In comparison with these methods, the performance of CEN-DMD outweights these methods. VisTex is a challenging texture dataset that contains textures with real scenes. Among all the comparison methods, LCVBP performs best and the classification accuracy rate exceeds 79%. The experimental results of CEN-DMD on the VisTex texture dataset are superior to other comparison methods. The USPTex texture dataset consists of real-world textures, including gravel, grass, tiles, and more. It can be seen from Table 3 that the LBP + LCC performs best in the comparison methods, and the classification accuracy rate exceeds 95%, but it is still lower than CEN-DMD by about 5%. The KTH-TIPS texture dataset contains texture changes in scale and illumination. The CEN-DMD classification accuracy rate is over 2.5% higher than the other methods.

It can be seen from Table 3 that although the classification accuracy of our proposed EN-DMD and CEN-DMD are close, we can still see subtle advantage. On the VisTex texture dataset, the classification accuracy of CEN-DMD has a slight advantage. On the CUReT and USPTex, the variance of CEN-DMD is smaller. The classification accuracy and variance on the Colored Brodatz are same. On the KTH-TIPS, the classification accuracy of EN-DMD has a slight advantage, but the variance of the two methods is the same.

In order to demonstrate the effectiveness of our proposed method, we compare it with the last texture characterization method, SWOBP [57], on CUReT and KTH-TIPS texture datasets. The experimental results are shown in Table 4. It can be seen from the Table 4 that our proposed method outperforms SWOBP with three sampling radius by 1%.

TABLE 4. The classification accuracy rate (%) compared with SWOBP on two datasets.

	CUReT	KTH-TIPS
SWOBP (R=1, P=8)	94.95	96.63
SWOBP (R=2, P=16)	96.72	97.56
SWOBP (R=3, P=24)	97.06	97.64
CEN-DMD	99.28	98.95

In addition, we compared with MICICM [58], [59] and GLCM_HSVCH [59], [60] on the more challenging texture dataset RawFoot. The RawFoot texture dataset consists of raw food samples such as meat, fish, grains and fruits, and contains changes in light direction, light source color and intensity. The RawFoot texture dataset used in the experiment contains all 69 texture classes, and each class consist 46 samples, of which 23 samples are used for training and 23 samples are used for testing. The size of each sample is 800 × 800 pixels. The experimental results are shown in Table 5. It can be seen from the Table 5 that the classification accuracy of our proposed CEN-DMD exceeds MICICM and GLCM_HSVCH on the RawFoot texture dataset.

TABLE 5. The classification accuracy rate (%) compared with MICICM and GLCM_HSVCH on RawFoot texture dataset.

	CUReT
MICICM	46.60
GLCM_HSVCH	34.97
CEN-DMD	88.75

To sum up, our proposed CEN-DMD is effective and outperforms the other thirteen representative texture classification methods on the five publicly available color texture datasets.

D. COMPARISONS WITH ORIGINAL DMD

In this subsection, we compared the our proposed method with the original DMD [42] on CUReT and KTH-TIPS texture datasets. The experimental results are shown in the Table 6. It can be seen from the table 6, the classification accuracy of our proposed EN-DMD and CEN-DMD exceeds the original DMD. It is demonstrated that texture descriptor that consider color information are more discriminative than texture descriptor captured only on grayscale image.

TABLE 6. The classification accuracy rates (%) compared with original DMD on two texture datasets.

	CUReT	KTH-TIPS
DMD	98.88	97.96
EN-DMD	99.24	98.98
CEN-DMD	99.28	98.95

E. RUNNING TIME

In this subsection, we compared the running time of different methods to extract one texture image feature by running MATLAB (R2014a) on a PC with Inter Core i5-7500 CPU and 8GB RAM. The experimental results are shown in Table 7. It can be seen from the Table 7 that the running time of our proposed CEN-DMD is only faster than Multilayer CCR. However, the classification performance of our proposed method is better.

TABLE 7. The running times (s) of different methods.

Method	CUReT (200×200)
IOCLBP	0.44
ECLMP	0.17
LBP+LCC	0.39
LCVBP	0.18
Multilayer CCR	1.48
OCLBP	0.11
ICM	0.26
ICM^{DFT}	0.36
OGF	0.65
CEN-DMD	0.89

V. CONCLUSION

In this paper, we propose a completed extremely nonnegative DMD (CEN-DMD) for color texture classification. CEN-DMD models the intrachannel information and interchannel information of color texture images by micro-block difference. In particular, during the difference process, we propose to nonnegative the difference features, and in order to capture the intrachannel and interchannel features simultaneously, the maximum of the intrachannel difference features and the maximum of the interchannel difference features are fused. Multiresolution representations of color texture are made by connecting micro-block difference features of different sizes. In addition, local micro-block difference features and global features of color texture are combined to construct CEN-DMD. Subsequently, the Fisher Vector is used to encode CEN-DMD to obtain a color texture descriptor. Finally, experimental results demonstrate that the proposed CEN-DMD outperforms the other thirteen representative color texture classification methods.

REFERENCES

[1] Y. Cong, D. Tian, Y. Feng, B. Fan, and H. Yu, "Speedup 3-D texture-less object recognition against self-occlusion for intelligent manufacturing," *IEEE Trans. Cybern.*, vol. 49, no. 11, pp. 3887–3897, Nov. 2019.
[2] J. Chan, Q. Kemao, and J. A. Lee, "Robust and efficient techniques for texture-less object recognition," in *Proc. Int. Workshop Adv. Image Technol. (IWAIT)*, Jan. 2018, pp. 1–4.
[3] J. Chan, J. A. Lee, and Q. Kemao, "BIND: Binary integrated net descriptors for texture-less object recognition," in *Proc. IEEE Conf. Comput. Vis. Pattern Recognit. (CVPR)*, Jul. 2017, pp. 2068–2076.
[4] C.-Y. Tsai and S.-H. Tsai, "Simultaneous 3D object recognition and pose estimation based on RGB-D images," *IEEE Access*, vol. 6, pp. 28859–28869, 2018.
[5] N. Werghi, C. Tortorici, S. Berretti, and A. Del Bimbo, "Boosting 3D LBP-based face recognition by fusing shape and texture descriptors on the mesh," *IEEE Trans. Inf. Forensics Security*, vol. 11, no. 5, pp. 964–979, May 2016.
[6] F. Hajati, M. Tavakolian, S. Gheisari, Y. Gao, and A. S. Mian, "Dynamic texture comparison using derivative sparse representation: Application to video-based face recognition," *IEEE Trans. Human-Mach. Syst.*, vol. 47, no. 6, pp. 970–982, Dec. 2017.
[7] X. Zhao, Y. Lin, and J. Heikkila, "Dynamic texture recognition using volume local binary count patterns with an application to 2D face spoofing detection," *IEEE Trans. Multimedia*, vol. 20, no. 3, pp. 552–566, Mar. 2018.
[8] K. Dimitropoulos, P. Barmpoutis, and N. Grammalidis, "Higher order linear dynamical systems for smoke detection in video surveillance applications," *IEEE Trans. Circuits Syst. Video Technol.*, vol. 27, no. 5, pp. 1143–1154, May 2017.
[9] A. Chadha, A. Abbas, and Y. Andreopoulos, "Video classification with CNNs: Using the codec as a spatio-temporal activity sensor," *IEEE Trans. Circuits Syst. Video Technol.*, vol. 29, no. 2, pp. 475–485, Feb. 2019.
[10] M. Kiechle, M. Storath, A. Weinmann, and M. Kleinsteuber, "Model-based learning of local image features for unsupervised texture segmentation," *IEEE Trans. Image Process.*, vol. 27, no. 4, pp. 1994–2007, Apr. 2018.
[11] S. Luo, L. Tong, and Y. Chen, "A multi-region segmentation method for SAR images based on the multi-texture model with level sets," *IEEE Trans. Image Process.*, vol. 27, no. 5, pp. 2560–2574, May 2018.
[12] Y. Dong, H. Zhang, Z. Liu, C. Yang, G.-S. Xie, L. Zheng, and L. Wang, "Neutrosophic set transformation matrix factorization based active contours for color texture segmentation," *IEEE Access*, vol. 7, pp. 93887–93897, 2019.
[13] M. Alkhatib and A. Hafiane, "Robust adaptive median binary pattern for noisy texture classification and retrieval," *IEEE Trans. Image Process.*, vol. 28, no. 11, pp. 5407–5418, Nov. 2019.
[14] A. Raza, H. Dawood, H. Dawood, S. Shabbir, R. Mehboob, and A. Banjar, "Correlated primary visual texton histogram features for content base image retrieval," *IEEE Access*, vol. 6, pp. 46595–46616, 2018.
[15] T. Ojala, M. Pietikainen, and T. Maenpaa, "Multiresolution gray-scale and rotation invariant texture classification with local binary patterns," *IEEE Trans. Pattern Anal. Mach. Intell.*, vol. 24, no. 7, pp. 971–987, Jul. 2002.
[16] Z. Guo, X. Wang, J. Zhou, and J. You, "Robust texture image representation by scale selective local binary patterns," *IEEE Trans. Image Process.*, vol. 25, no. 2, pp. 687–699, Feb. 2016.
[17] L. Ji, Y. Ren, G. Liu, and X. Pu, "Training-based gradient LBP feature models for multiresolution texture classification," *IEEE Trans. Cybern.*, vol. 48, no. 9, pp. 2683–2696, Sep. 2018.
[18] Y. El Merabet, Y. Ruichek, and A. El Idrissi, "Attractive-and-repulsive center-symmetric local binary patterns for texture classification," *Eng. Appl. Artif. Intell.*, vol. 78, pp. 158–172, Feb. 2019.
[19] T. Wang, Y. Dong, C. Yang, L. Wang, L. Liang, L. Zheng, and J. Pu, "Jumping and refined local pattern for texture classification," *IEEE Access*, vol. 6, pp. 64416–64426, 2018.
[20] Y. Dong, T. Wang, C. Yang, L. Zheng, B. Song, L. Wang, and M. Jin, "Locally directional and extremal pattern for texture classification," *IEEE Access*, vol. 7, pp. 87931–87942, 2019.
[21] Y. El Merabet and Y. Ruichek, "Local concave-and-convex micro-structure patterns for texture classification," *Pattern Recognit.*, vol. 76, pp. 303–322, Apr. 2018.
[22] Z. Guo, L. Zhang, and D. Zhang, "A completed modeling of local binary pattern operator for texture classification," *IEEE Trans. Image Process.*, vol. 19, no. 6, pp. 1657–1663, Jun. 2010.
[23] L. Liu, Y. Long, P. W. Fieguth, S. Lao, and G. Zhao, "BRINT: Binary rotation invariant and noise tolerant texture classification," *IEEE Trans. Image Process.*, vol. 23, no. 7, pp. 3071–3084, Jul. 2014.
[24] L. Liu, S. Lao, P. W. Fieguth, Y. Guo, X. Wang, and M. Pietikäinen, "Median robust extended local binary pattern for texture classification," *IEEE Trans. Image Process.*, vol. 25, no. 3, pp. 1368–1381, Mar. 2016.
[25] Y. Dong and J. Ma, "Wavelet-based image texture classification using local energy histograms," *IEEE Signal Process. Lett.*, vol. 18, no. 4, pp. 247–250, Apr. 2011.
[26] Y. Dong, J. Feng, L. Liang, L. Zheng, and Q. Wu, "Multiscale sampling based texture image classification," *IEEE Signal Process. Lett.*, vol. 24, no. 5, pp. 614–618, May 2017.
[27] Y. Dong and J. Ma, "Feature extraction through contourlet subband clustering for texture classification," *Neurocomputing*, vol. 116, pp. 157–164, Sep. 2013.
[28] Y. Dong, D. Tao, X. Li, J. Ma, and J. Pu, "Texture classification and retrieval using shearlets and linear regression," *IEEE Trans. Cybern.*, vol. 45, no. 3, pp. 358–369, Mar. 2015.

[29] Y. Dong, D. Tao, and X. Li, "Nonnegative multiresolution representation-based texture image classification," *ACM Trans. Intell. Syst. Technol.*, vol. 7, no. 1, pp. 1–21, Oct. 2015.

[30] Y. Dong and J. Ma, "Bayesian texture classification based on contourlet transform and BYY harmony learning of Poisson mixtures," *IEEE Trans. Image Process.*, vol. 21, no. 3, pp. 909–918, Mar. 2012.

[31] B. S. Manjunath, J.-R. Ohm, V. V. Vasudevan, and A. Yamada, "Color and texture descriptors," *IEEE Trans. Circuits Syst. Video Technol.*, vol. 11, no. 6, pp. 703–715, Jun. 2001.

[32] U. Kandaswamy, D. A. Adjeroh, S. Schuckers, and A. Hanbury, "Robust color texture features under varying illumination conditions," *IEEE Trans. Syst. Man, Cybern. B, Cybern.*, vol. 42, no. 1, pp. 58–68, Feb. 2012.

[33] J. J. de Mesquita Sa Junior, P. C. Cortez, and A. R. Backes, "Color texture classification using shortest paths in graphs," *IEEE Trans. Image Process.*, vol. 23, no. 9, pp. 3751–3761, Sep. 2014.

[34] F. Bianconi, R. Bello-Cerezo, and P. Napoletano, "Improved opponent color local binary patterns: An effective local image descriptor for color texture classification," *J. Electron. Imag.*, vol. 27, no. 1, Dec. 2017, Art. no. 011002.

[35] F. Riaz, A. Hassan, R. Nisar, M. Dinis-Ribeiro, and M. T. Coimbra, "Content-adaptive region-based color texture descriptors for medical images," *IEEE J. Biomed. Health Informat.*, vol. 21, no. 1, pp. 162–171, Jan. 2017.

[36] Y. Chen, D. Li, and J. Q. Zhang, "Complementary color wavelet: A novel tool for the color image/video analysis and processing," *IEEE Trans. Circuits Syst. Video Technol.*, vol. 29, no. 1, pp. 12–27, Jan. 2019.

[37] F. Bianconi, R. W. Harvey, P. Southam, and A. Fernández, "Theoretical and experimental comparison of different approaches for color texture classification," *J. Electron. Imag.*, vol. 20, no. 4, Oct. 2011, Art. no. 043006.

[38] R. Bello-Cerezo, F. Bianconi, F. Di Maria, P. Napoletano, and F. Smeraldi, "Comparative evaluation of hand-crafted image descriptors vs. Off-the-shelf CNN-based features for colour texture classification under ideal and realistic conditions," *Appl. Sci.*, vol. 9, no. 4, p. 738, Feb. 2019.

[39] C. Li, Y. Huang, and L. Zhu, "Color texture image retrieval based on Gaussian copula models of Gabor wavelets," *Pattern Recognit.*, vol. 64, pp. 118–129, Apr. 2017.

[40] X. Li and K. N. Plataniotis, "Color texture representation using circular-processing based hue-LBP for histo-pathology image analysis," in *Proc. IEEE Int. Conf. Image Process. (ICIP)*, Sep. 2016, pp. 3573–3577.

[41] F. Lehmann, "Turbo segmentation of textured images," *IEEE Trans. Pattern Anal. Mach. Intell.*, vol. 33, no. 1, pp. 16–29, Jan. 2011.

[42] R. Mehta and K. Egiazarian, "Texture classification using dense micro-block difference," *IEEE Trans. Image Process.*, vol. 25, no. 4, pp. 1604–1616, Apr. 2016.

[43] Y. Dong, H. Wu, X. Li, C. Zhou, and Q. Wu, "Multiscale symmetric dense micro-block difference for texture classification," *IEEE Trans. Circuits Syst. Video Technol.*, vol. 29, no. 12, pp. 3583–3594, Dec. 2019.

[44] R. C. Gonzalez and R. E. Woods, *Digital Image Processing*, 4th ed. London, U.K.: Pearson, 2017.

[45] J. Sánchez, F. Perronnin, T. Mensink, and J. Verbeek, "Image classification with the Fisher vector: Theory and practice," *Int. J. Comput. Vis.*, vol. 105, no. 3, pp. 222–245, Dec. 2013.

[46] F. Perronnin, J. Sánchez, and T. Mensink, "Improving the Fisher kernel for large-scale image classification," in *Proc. Eur. Conf. Comput. Vis. (ECCV)*, in Lecture Notes in Computer Science, vol. 6314. Berlin, Germany: Springer, 2010, pp. 143–156.

[47] T. T. Negri, F. Zhou, Z. Obradovic, and A. Gonzaga, "Extended color local mapped pattern for color texture classification under varying illumination," *J. Electron. Imag.*, vol. 27, no. 1, Feb. 2018, Art. no. 011008.

[48] S. R. Dubey, S. K. Singh, and R. K. Singh, "Multichannel decoded local binary patterns for content-based image retrieval," *IEEE Trans. Image Process.*, vol. 25, no. 9, pp. 4018–4032, Sep. 2016.

[49] C. Cusano, P. Napoletano, and R. Schettini, "Combining local binary patterns and local color contrast for texture classification under varying illumination," *J. Opt. Soc. Amer. A, Opt. Image Sci.*, vol. 31, no. 7, pp. 1453–1461, 2014.

[50] S. H. Lee, J. Y. Choi, Y. M. Ro, and K. N. Plataniotis, "Local color vector binary patterns from multichannel face images for face recognition," *IEEE Trans. Image Process.*, vol. 21, no. 4, pp. 2347–2353, Apr. 2012.

[51] F. Bianconi, A. Fernández, E. González, D. Caride, and A. Calviño, "Rotation-invariant colour texture classification through multilayer CCR," *Pattern Recognit. Lett.*, vol. 30, no. 8, pp. 765–773, Jun. 2009.

[52] M. E. Barilla and M. Spann, "Colour-based texture image classification using the complex wavelet transform," in *Proc. 5th Int. Conf. Electr. Eng., Comput. Sci. Autom. Control*, Nov. 2008, pp. 358–363.

[53] T. Mäenpää and M. Pietikäinen, "Texture analysis with local binary patterns," in *Handbook of Pattern Recognition and Computer Vision*. Singapore: World Scientific, 2005, pp. 197–216.

[54] V. Arvis, C. Debain, M. Berducat, and A. Benassi, "Generalization of the cooccurrence matrix for colour images: Application to colour texture classification," *Image Anal. Stereology*, vol. 23, no. 1, pp. 63–72, 2004.

[55] A. Jain and G. Healey, "A multiscale representation including opponent color features for texture recognition," *IEEE Trans. Image Process.*, vol. 7, no. 1, pp. 124–128, Jan. 1998.

[56] R. Bello-Cerezo, F. Bianconi, A. Fernández, E. González, and F. Di Maria, "Experimental comparison of color spaces for material classification," *J. Electron. Imag.*, vol. 25, no. 6, Jun. 2016, Art. no. 061406.

[57] T. Song, J. Feng, S. Wang, and Y. Xie, "Spatially weighted order binary pattern for color texture classification," *Expert Syst. Appl.*, vol. 147, Jun. 2020, Art. no. 113167.

[58] B. Khaldi and M. L. Kherfi, "Modified integrative color intensity co-occurrence matrix for texture image representation," *J. Electron. Imag.*, vol. 25, no. 5, Sep. 2016, Art. no. 053007.

[59] B. Khaldi, O. Aiadi, and M. L. Kherfi, "Combining colour and grey-level co-occurrence matrix features: A comparative study," *IET Image Process.*, vol. 13, no. 9, pp. 1401–1410, Jul. 2019.

[60] K. Ch, R. B. Prabhakara, and D. Govardhan, "Image retrieval based on color and texture features of the image sub-blocks," *Int. J. Comput. Appl.*, vol. 15, no. 7, pp. 2237–2245, Feb. 2011.

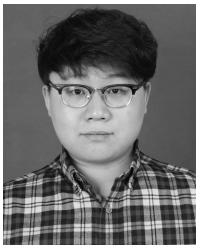

MINGXIN JIN is currently pursuing the M.S. degree with the School of Information Engineering, Henan University of Science and Technology, China. His current research interests include pattern recognition, machine learning, and computer vision.

YONGSHENG DONG (Senior Member, IEEE) received the Ph.D. degree in applied mathematics from Peking University, in 2012.

From 2013 to 2016, he was a Postdoctoral Research Fellow with the Center for Optical Imagery Analysis and Learning, Xi'an Institute of Optics and Precision Mechanics, Chinese Academy of Sciences, Xi'an, China. From 2016 to 2017, he was a Visiting Research Fellow with the School of Computer Science and Engineering, Nanyang Technological University, Singapore. He has authored or coauthored over 40 articles at famous journals and conferences, including the IEEE TRANSACTIONS ON IMAGE PROCESSING, the IEEE TRANSACTIONS ON NEURAL NETWORKS AND LEARNING SYSTEMS, the IEEE TRANSACTIONS ON CYBERNETICS, the IEEE TRANSACTIONS ON INDUSTRIAL ELECTRONICS, the IEEE TRANSACTIONS ON CIRCUITS AND SYSTEMS FOR VIDEO TECHNOLOGY, and ACM TIST. His current research interests include pattern recognition, machine learning, and computer vision. He is an Associate Editor of *Neurocomputing*.

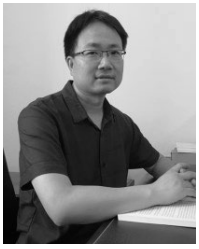

MINGCHUAN ZHANG (Member, IEEE) received the Ph.D. degree in communication and information system from the Beijing University of Posts and Telecommunications, in July 2014. He is currently an Associate Professor with the School of Information Engineering, Henan University of Science and Technology, China. His research interests include the future Internet, machine learning, and optimization. He is a member of the China Computer Federation (CCF) and a Senior Member of the Chinese Association of Artificial Intelligence (CAAI).

QINGTAO WU is currently a Full Professor with the School of Information Engineering, Henan University of Science and Technology, China. His research interests include computer security, the future Internet security, machine learning, and cloud computing. He is a member of the China Computer Federation (CCF) and a Senior Member of the Chinese Association of Artificial Intelligence (CAAI).

LINTAO ZHENG received the Ph.D. degree in computer science from Zhejiang University, in 2012. He is currently a Lecturer with the School of Information Engineering, Henan University of Science and Technology, Luoyang, China. His current research interests include image processing and computer vision.

BIN SONG received the B.S. degree in computer science from Zhengzhou University, in 2003, the M.Sc. degree in computer science from the China University of Geosciences, in 2007, and the Ph.D. degree in computer science from Korea University, in 2016. He is currently a Lecturer with the Henan University of Science and Technology. His research interests include pattern recognition, image processing, and computer vision.

LEI ZHANG is currently a Lecturer with the School of Information Engineering, Henan University of Science and Technology, Luoyang, China. Her current research interests include image processing and computer vision.

LIN WANG received the Ph.D. degree in image and signal processing from INSA de lyon, France, in 2016. She is currently a Lecturer with the Information College, Henan University of Science and Technology, Luoyang, China. Her current research interests include image processing and computer vision.